VOID MINIMIZATION AND OPTIMIZATION OF INJECTION VELOCITY IN RTM PROCESSING

C. Ravey, F. Lebel, E. Ruiz, H.Courteau-Godmaire, F. Trochu*

Department of Mechanical Engineering, Chair on Composites of High Performance (CCHP), Centre de Recherche sur les Polymères et Composites à haute performance (CREPEC),

École Polytechnique de Montréal, Station « Centre-Ville », Montréal, Canada, H3C 3A7

* Corresponding author (trochu@polymtl.ca)

***Keywords**: RTM, optimal velocity, glass fibers, capillary rise, voids content, saturation*

1 Introduction

Liquid Composite Molding (LCM) is an increasingly used class of processes to manufacture high performance composites [1-3]. In Resin Transfer Molding (RTM), a reactive liquid resin is injected inside a mold cavity containing a dry fibrous reinforcement. In order to produce high performance composites, the fibers must be completely saturated prior to resin gelation [4]. Indeed, impregnation defects have a detrimental impact on the mechanical properties of composite parts such as the maximum compression, flexural and shear inter-laminar strengths [5, 6].

The engineering fabrics in LCM possess generally a dual scale architecture in terms of porosity. Microscopic pores exist between the filaments inside the fiber tows, while macroscopic pores appear between the tows. As a result, microvoids are formed inside the fibers tows for low injection velocity, and macroscopic voids appear between the fibers tows when the injection velocity is high [7-9]. Several approaches can be considered to minimize the void content, such as bleeding after mold filling or applying a consolidation pressure. However, these methods are expensive and are not well adapted to complex geometry or large parts. Hence, developing practical strategies to produce composites with a high impregnation quality becomes a critical industrial goal [10].

The capillary rise method has been used to characterize the permeability, the architecture of porous media and the capillary pressure at equilibrium in different soils. Researchers have also studied by this approach the microscopic and macroscopic properties of fibrous reinforcements used in high performance composites [11, 12]. However, for composite materials, this characterization technique suffered from a lack of precision, repeatability and robustness [11-14].

To circumvent these technical limitations, a monitoring technique based on fluorescent *Dye Penetration Inspection* (*DPI*) and CCD image acquisition has been developed [15, 16]. This visual monitoring of the capillary front by fluorescence is coupled with real time fluid mass acquisition with a high resolution balance. This allows gathering automatically and simultaneously the capillary front position and the uptake fluid mass in time with a high degree of accuracy and repeatability.

The goal of this investigation is to find a way to predict the optimal injection velocity for a given fabric and resin using capillary rise measurements. The first part of this paper is devoted to modelling the capillary rise phenomenon in fabrics of dual scale porosity, and then the model is used to predict the optimal injection velocity. Note that the capillary rise measurement method with DPI was improved by following new experimental protocols and using image processing techniques to follow the progression of the capillary front. Finally, the whole procedure is validated by simulating injections in parts of irregular geometry, in which the injection velocity is monitored to maintain the optimal velocity of the flow front.

2. The capillary rise method

2.1 Experimental setup

The principle of capillary rise measurements is fairly simple: it consists of dipping a fabric sample in resin or in a probe fluid in order to study the wetting, wicking and imbibition behavior of the liquid in the porous medium. In the present work, a capillary rise setup has been developed to record simultaneously the flow front position and the uptake fluid mass. The experimental setup is shown in Fig. 1. It is composed of a 14.1 megapixels digital camera from *Canon*® and a high resolution scale. The digital camera was remotely controlled and each capture of the capillary rise progression was taken at a specific rate of 1 image per 5 seconds. The liquid containers are standard rheometer capsules. The high surface area of the liquid containers with respect to the total fluid uptake volume absorbed by the fiber tows allows minimizing buoyancy force variations during wicking as a result of the decrease in the liquid level.

In order to control the fiber tow velocity when it comes in contact with the liquid surface, a motorized linear stage moves the fabric samples held on a frame. A control software was developed to stop the motor once the fiber tow touches the liquid surface (which translates in a mass jump on the scale reading). Two 15 Watts UV-black light bulbs were used to follow the progression of the fluid with the fluorescent dye.

2.2 Modeling of flows during capillary rise

Several models exist to analyze the progression of the capillary front in fiber tows. A simplified approach is presented here. During isothermal capillary rise experiments in immobile, non stretchable and tortuous fiber tows, the fluids used are considered incompressible and Newtonian. In this respect, Fig. 2 shows the typical capillary height evolution in time of such a liquid through a porous medium. The progression of the capillary front tends asymptotically towards an equilibrium height z_{eq}, for which the capillary and gravitational forces balance each other in static equilibrium. Fig. 2 highlights also the linear flow regime of *Lucas-Washburn* for which the gravity contribution can be neglected at the beginning of the experiment. In that situation, capillary forces are balanced only by viscous forces.

By summing up along the z direction the forces driving a *Hagen-Poiseuille* flow in a tortuous fiber bundle, the balance of capillary, gravity and viscous forces gives the following equation [17]:

$$\underbrace{\pi \frac{d_h^2}{4} \rho \tau^2 \, z \frac{d^2 z}{dt^2}}_{\text{inertia}} = \underbrace{\pi \frac{d_h^2}{4} P_{cap}}_{\text{capillarity}} - \underbrace{8\pi\mu\tau^2 \, z \frac{dz}{dt}}_{\text{viscous drag}} - \underbrace{\pi \frac{d_h^2}{4} \rho g \, z}_{\text{gravity}} \quad (1)$$

where d_h is the hydraulic diameter of the fluid flow (m), ρ the density of the fluid (kg.m^{-3}), τ the tortuosity of the fibers bundle (generally τ tends to be close to 1), P_{cap} the capillary pressure (Pa) given by Laplace equation, μ the viscosity of the fluid (Pa.s) and g is the gravity acceleration (m.s^{-2}).

Inertia and gravity contribution can be neglected on short distances($z << z_{eq}$). Using the modified *Jurin*'s law [18] to express the capillary pressure, equation (1) can be simplified as follows :

$$0 = \pi \frac{d_h^2}{4} \underbrace{\rho g \, z_{eq}}_{P_{cap}} - 8\pi\mu\tau^2 \, z \frac{dz}{dt} \quad (2)$$

from which an ordinary differential equation (ODE) describing the axial progression in time of the capillary height in fiber tows is obtained, as expressed in the following:

$$\frac{dz}{dt} = \beta_h \left(\frac{z_{Jurin}}{z} \right) \quad (3)$$

where

$$\beta_h = \frac{d_h^2 \rho g}{32 \mu \tau^2} \quad (4)$$

The integration of equation (3) results in the classical *Lucas-Washburn* imbibition model giving the evolution of the capillary height on short imbibition distances as follows :

$$z^2 = B_h \, t \quad (5)$$

where

$$B_h = 2 \beta_h \, z_{Jurin} \quad (6)$$

The parameter B_h represents the *Lucas-Washburn* (*LW*) slope of the square of the capillary height during the linear *Lucas-Washburn* flow regime (*i.e*, on short imbibition distances). This term, which was also referred to as a diffusion or capillary rate

coefficient (m^2/s) [19], can be obtained by linear regression.

2.3 Image post-treatment

After a capillary rise test, the images recorded at constant time step are post-processed by a *Matlab* program. The initial routine [15, 16] was developed as follows :

1. Fluorescent-colored RGB pictures are converted into gray levels by Hue-Saturation-Intensity (*HIS*) algorithm.
2. In order to track the capillary front, the program performs a binary conversion based on *Otsu*'s thresholding algorithm.
3. Finally, edge filtering is applied on binary pictures in order to discard noisy pixels. The pixels are removed on each pixel column except the pixel of maximum height.

This semi-automated strategy was found to be quite robust and efficient to track the capillary front despite the variable brightness of the recorded images. Two factors contribute to this variable brightness: (1) the variable shutter speed of the semi-automatic camera; and (2) the total increase in brightness resulting from the use of fluorescent liquids. Fig. 3 illustrates the tracking process on images of the capillary front: Fig. 3a shows a typical raw image, while Fig. 3b displays the successive average front positions evaluated at each time step from the pixel images by *Otsu*'s algorithm and edge filtering.

3. Optimization of the capillary rise method

Despite the efficiency of the previously described method for fiber tows, a small shift is detected with the real capillary front in fabric samples. Indeed, the dual scale architecture of the reinforcement brings in the so-called "*fingering*" effect [20-22], *i.e.* the front inside the fiber tows is usually ahead of front in between the tows (see Fig. 6a). Some experimental and numerical adjustments are required in order to overcome this source of error when detecting the positions of the capillary front, especially in fabric samples.

First of all, the whole experimental setup was placed in an isolated enclosed dark room in order to prevent perturbations coming from an external light source, air streams and vibrations on the mass and image acquisitions. All the equipment (motor, balance, and camera) are controlled with a computer placed inside the dark room. This computer is itself remotely controlled from outside the dark room via internet to prevent any disturbance during the launch of the experiments.

In order to minimize the brightness problems mentioned, the experimental setup was equipped with a new high resolution camera with a full frame captor and the possibility to control the brightness level in manual mode. These features allowed collecting more accurate data and hence improving the image post-processing to better locate the capillary front.

Otsu's threshold algorithm is a powerful tool to convert gray levels to binary black and white images. However, the threshold can vary from one image to another. For this reason, a new conversion function adapted to capillary images was proposed. The gray signal from Fig. 4 is averaged in the *x* direction and plotted against the *y* direction for every images captured during the capillary rise (see Fig. 5). Each curve is the result of a different image, all of which are taken at intervals of 5 seconds.

The wet part of the fabric sample is on the left side of the curves, and the dry part on the right. Thanks to the camera settings, it is possible to see that the minimum and maximum values of the signal remain constant in time. The threshold between black and white pixels is set by the user and expressed as a percentage of magnitude between the maximum and minimum values of the gray signal. The same threshold is then applied to every image. This method provides a simple and efficient way to control the threshold for a set of images during capillary rise experiments. Thanks to these experimental and numerical adjustments, it was possible to estimate the velocity of the capillary front with a better accuracy.

As shown in Fig. 6, the front detected with *Otsu*'s algorithm does not correspond to the positions given by the new approach, which is closer to the peaks inside the fiber tows. Thus, the height *z* (mm) of the liquid can be evaluated on each frame.

4 Prediction of optimal injection velocity for 2D glass fibers fabrics

The void content is generally plotted as a function of the capillary number, or better of the modified capillary number below, which takes into account the contact angle θ between the fluid and the fabric:

$$Ca^* = \frac{\mu \, .v}{\gamma \ \cos\theta} \tag{7}$$

where μ is the viscosity of the liquid (Pa.s), v the velocity of the flow front (m.s^{-1}) and γ the surface tension (N.m^{-1}) of the fluid. As shown in Fig. 7, the typical evolution of void content as a function of the capillary number exhibits a "V-shaped" curve [8, 20]. The objective is to determine the optimum capillary number, for which a minimum void content is achieved at the bottom of the "V-shaped curve". For that purpose, capillary rise tests are conducted to identify the left side of the "V-shaped curve" for low velocity flows.

Capillary rise experiments have shown that the spontaneous imbibition velocity corresponds to a minimum macroscopic void content. Thus, the optimal velocity can be evaluated as the velocity for which an elementary cell of characteristic size L_c is filled up with fluid. If t_c, denotes the characteristic time required to fill an elementary cell in spontaneous capillary impregnation, then the optimal impregnation velocity (see Fig. 8) may be defined as follows:

$$v_{opt} = \frac{L_c}{t_c} \tag{8}$$

Using the Lucas Washburn model of equation (5), we get :

$$L_c^{\ 2} = B_h \ t_c \tag{9}$$

Combining equations (8) and (9) allows expressing the optimal velocity as a function of two known parameters, the characteristic length L_c (measured directly on the fabric) and the Lucas Washburn slope B_h, as follows :

$$v_{opt} = \frac{B_h}{L_c} \tag{10}$$

Parameter B_h is determined from image processing as described in the previous section. Firstly, the image treatment allows calculating and plotting the fluid height as a function of time. As shown in Fig. 9, the results for several capillary rise tests in the warp and weft directions for the JB Martin TG15N NCF fiber glass fabrics gave repeatable and stable results. As expected from the theoretical curve of Fig. 2, the height tends to stabilize itself after a long period of time. Secondly, the square height is plotted against time only on short times (t < 50 s) so that gravitational effects can be considered as negligible. As shown in Fig. 10, a linear evolution is observed. Thus the Lucas Washburn model is verified. From these data, it is possible to determine B_h. The value of B_h is strongly dependent on the number of time steps taken for the linear regression. Indeed, it is possible to notice in Fig. 10 that the slope between t = 0 and t = 10s is greater than the slope between t = 0 and t = 50 s. The influence of the number of time steps on B_h was studied and is shown in Fig. 11. Since the three different tests in each warp and weft direction are repeatable, a mean value of these three tests was taken for the sequel of this investigation.

In Fig. 11, we see that the value of B_h decreases rapidly with the number of time steps. Before 50 s, the values of B_h are too high because the number of time steps in the linear regression is too low to give a representative value as the slope varies too much between time steps. After 50 s, the value of B_h is less affected by the number of time steps and the R^2 coefficient of the linear regression remains acceptable. Thus, the value of B_h can be taken at t = 50 s as a preliminary result. The influence of B_h on the optimal velocity will also be further investigated.

The characteristics length L_c is determined experimentally by taking HD images with the same camera used for capillary tests and macro lens. HD pictures are taken on a 2 x 2 inches square fabric sample. This allows performing more than 20 measurements and provides a statistical analysis on L_c results. This turns out to be a fast, cost effective and accurate way of evaluating L_c.

The results of B_h, L_c and the calculation of v_{opt} for the hexadecane are presented in Table 1. These values of velocity for hexadecane need to be converted in equivalent velocity for resin injections.

The modified capillary number defined in equation (7) remains constant for different fluids in the same fabrics. Thus, it is possible from the properties of the resin to calculate the equivalent optimal resin

velocity as expressed below, without having to carry out capillary tests with resin:

$$v_{resin} = Ca^{*}.\frac{\gamma_{resin}\cos\theta_{resin}}{\mu_{resin}} \qquad (11)$$

The surface tension, viscosity and contact angle are known from previous experiments [23]. The velocity calculated for two resins, the vinyl ester 411-350 from *Derakane®* and the epoxy DER 383 from *Dow®* (see Table 2) is in good agreement with the values given in previous investigations. Indeed, for each resin and in each direction, the velocity value from the present work is within the range of velocities defined by LeBel *et al*.

The values in Table 2 are obtained for a mean value of Bh taken at t = 50s (see Fig. 11). However, the calculation of the optimal velocity depends on the value of Bh The resin optimal velocity was calculated by equation (11) as a function of Bh The results presented in Fig. 12 show that the estimated velocity varies linearly with Bh The values located on the right end of the lines correspond to the initial estimation (with a few time steps). Then, as the time steps increases, the estimated velocity tends to group on the left end of the lines. The optimal range can be defined by this group of values on the left end of the lines, when the Bh.parameter stabilizes in the Lucas Washburn model.

The optimal injection velocity ranges having been determined from capillary rise experiments, it is now possible to validate this approach by evaluating the optimal velocity from the analysis of void content in composite samples fabricated by resin injection.

5. Simulation of RTM injections in composite samples of uniform and variable width

Composites samples were fabricated by resin injection with JB Martin TG15N NCF glass fiber fabrics and vinyl ester resin. Firstly, injection simulations were carried out with PAM-RTM software in order to analyze the flow behavior and estimate the void content.

Two different geometries have been studied: a rectangular plate of uniform width (Fig. 13a) and a section constriction in the same plate (Fig. 13b). The idea is to validate the optimal velocity in the plate of uniform width and then try to monitor the velocity on a more complex geometry.

The real injections will be carried out with 6 plies of JB Martin TG15N glass fiber fabric in a mold cavity of 3.175 mm in thickness, which corresponds to a fiber volume fraction V_f of approximately 38%. The geometry and mesh was generated with CATIA And the numerical simulations performed at constant flow rate. The small section the constriction plate is twice smaller than in the larger part. Thus, when the optimal velocity v_{opt} is monitored in the large section, the resulting velocity in the small section will be equal to 2 v_{opt}. Inversely, when the optimal velocity v_{opt} is monitored in the small section, the resulting velocity in the large section is 0.5 v_{opt}. The last simulation consists of monitoring the optimal velocity is both sections, which will result in a decrease of the flow rate in the small section.

The void contents obtained in the simulations are presented in Table 3 and Fig. 14. As expected, the void content is minimal for the optimal injection velocity. Moreover, when the optimal velocity is monitored in the two sections, the minimum void content is also maintained. The typical “V-shaped” curve is clearly visible in Fig. 14. The macroscopic voids are located on the left side of the “V”, whereas microscopic voids appear on the right. As already observed in the scientific literature [7-9], the void content increases more rapidly at lower injection velocity, forming an asymmetrical “V-shaped” trend.

These simulations results prove the importance of monitoring the injection velocity during RTM processing. Capillary rise tests allow to estimate the optimal injection velocity. The real injections will be performed on a semi industrial scale setup. This experimental setup has already been used to fabricate rectangular plates of uniform width by resin injection [24]. The flow rate will be monitored via an automated user interface. Then, samples from the injected parts will be cut for void content analysis.

6. Conclusion

In the present work, capillary rise experiments were performed to visualise the impregnation of fiber glass fabrics by a reference fluid (hexadecane). The experimental procedure was enhanced by using a fluorescence technique with HD optical means in order to record images of liquid imbibition during the capillary rise. The post-treatment of experimental data was also improved with a fast and efficient way based on image processing to locate the fluid front during capillary rise tests. The Lucas Washburn model could then be used to estimate the optimal injection velocity. The main advantage of this approach lies in the possibility of calculating the equivalent resin optimal velocity from the modified capillary number without carrying out capillary tests with resins. However, this experimental procedure is only valid for transparent fabrics made of glass fibers for example.

Once the optimal injection velocity was determined by capillary tests, the results were validated by numerical simulations carried out with PAM-RTM software. The study of resin injection in composite samples of variable geometry shows that the estimated optimal velocity gives the lowest voids content. The numerical simulations permit also to retrieve the typical void distribution as a function of injection velocity. The next step consists of injecting real composite samples in order to confirm the simulation results.

Since this approach is valid only in transparent fabrics made out of glass fibers, future work will focus on finding the optimal injection velocity in non-transparent fabrics such as carbon fibers. Two options will be considered: (1) analysing the mass data measured with the balance; (2) changing the image acquisition method from ultraviolet fluorescence to infrared recording.

Acknowledgments

The authors would like to thank the National Science and Engineering Research Council (NSERC) of Canada and the Fonds Québécois pour la Recherche sur la Nature et les Technologies (FQRNT) and the Canada Research Chairs for their financial support. The contributions of Canada Foundation for Innovation (CFI) and of Safran to the research infrastructure are gratefully acknowledged, as well as the technical assistance of Christian-Charles Martel.

References

[1]. Gay, D. and S.V. Hoa "*Composite Materials: Design And Applications*". CRC Press, 2007

[2]. Chung, D.D.L. "*Composite Materials: Science and Applications*". Springer London, 2010

[3]. Parnas, R.S. "*Liquid Composite Molding*". Carl Hanser GmbH, 2000

[4]. Trochu, F., E. Ruiz, V. Achim, and S. Soukane "Advanced numerical simulation of liquid composite molding for process analysis and optimization". *Composites Part A: Applied Science and Manufacturing*, 37(6), p. 890-902, 2006.

[5]. Leclerc, J.S. and E. Ruiz "Porosity reduction using optimized flow velocity in Resin Transfer Molding". *Composites Part A: Applied Science and Manufacturing*, 39(12), p. 1859-1868, 2008.

[6]. Ghiorse, S.R. "Effect of void content on the mechanical properties of carbon/epoxy laminates". *SAMPE Quarterly*, 24(2), 1993.

[7]. Ruiz, E., V. Achim, S. Soukane, F. Trochu, et al. "Optimization of injection flow rate to minimize micro/macro-voids formation in resin transfer molded composites". *Composites Science and Technology*, 66(3-4), p. 475-486, 2006.

[8]. Patel, N. and L.J. Lee "Modeling of void formation and removal in liquid composite molding. Part II: Model development and implementation". *Polymer Composites*, 17(1), p. 104-114, 1996.

[9]. Patel, N. and L.J. Lee "Modeling of void formation and removal in liquid composite molding. Part I: Wettability analysis". *Polymer Composites*, 17(1), p. 96-103, 1996.

[10]. Achim, V. and E. Ruiz "Guiding selection for reduced process development time in

RTM". *International Journal of Material Forming*, 3(S2), p. 1277-1286, 2009.

[11]. Amico, S.C. and C. Lekakou "Axial impregnation of a fiber bundle. Part 1: Capillary experiments". *Polymer Composites*, 23(2), p. 249-263, 2002.

[12]. Amico, S.C. and C. Lekakou "Axial impregnation of a fiber bundle. Part 2: Theoretical analysis". *Polymer Composites*, 23(2), p. 264-273, 2002.

[13]. Hsieh, Y.-L. and B. Yu "Liquid Wetting, Transport, and Retention Properties of Fibrous Assemblies: Part I: Water Wetting Properties of Woven Fabrics and Their Constituent Single Fibers". *Textile Research Journal*, 62(11), p. 677-685, 1992.

[14]. Bayramli, E. and R.L. Powell, *Experimental Investigation Of The Axial Impregnation Of Oriented Fiber Bundles By Capillary Forces*, 1992, U.S Army Laboratory Command.

[15]. LeBel, F., A.E. Fanaei, É. Ruiz, and F. Trochu "Experimental Characterization by Fluorescence of Capillary Flows in the Fiber Tows of Engineering Fabrics". *Open Journal of Inorganic Non-metallic Materials*, 02(03), p. 25-45, 2012.

[16]. LeBel, F., A.E. Fanaei, E. Ruiz, and F. Trochu "Experimental characterization by fluorescence of capillary flows in dual-scale engineering fabrics". *Textile Research Journal*, 2013.

[17]. Johnson, R.W. "*The Handbook Fluid Dynamics*". Crc Press, 1998

[18]. de Gennes, P.G., F. Brochard-Wyart, and D. Quere "*Capillarity and Wetting Phenomena: Drops, Bubbles, Pearls, Waves*". Springer, 2010

[19]. Hamdaoui, M., F. Fayala, and S.B. Nasrallah "Dynamics of capillary rise in yarns: Influence of fiber and liquid characteristics". *Journal of Applied Polymer Science*, 104(5), p. 3050-3056, 2007.

[20]. Labat, L., J. Breard, S. Pillut-Lesavre, and G. Bouquet "Void fraction prevision in LCM parts". *EPJ Applied Physics*, 16(2), p. 157-164, 2001.

[21]. Duan Yuexin, Z.L., Zhao Yan, Zhang Zuoguang, Liang Zhiyong, *Effect Of Fabric Structure On Deffects In Composites Manufactured By RTM*, in *ICCM 16*2007: Kyoto, Japan.

[22]. Pearce, N., F. Guild, and J. Summerscales "A study of the effects of convergent flow fronts on the properties of fibre reinforced composites produced by RTM". *Composites Part A: Applied Science and Manufacturing*, 29(1–2), p. 141-152, 1998.

[23]. LeBel, F., A.E. Fanaei, É. Ruiz, and F. Trochu "Prediction of optimal flow front velocity to minimize void formation in dual scale fibrous reinforcements". *International Journal of Material Forming*, 2012.

[24]. LeBel, F., *Contrôle de la fabrication des composites par injection sur renforts*, PhD thesis, *Département de génie mécanique*, École Polytechnique de Montréal. 2012.

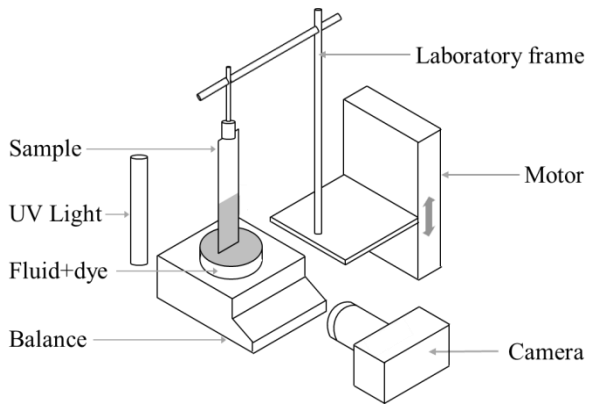

Fig. 1: Experimental setup for capillary rise measurements.

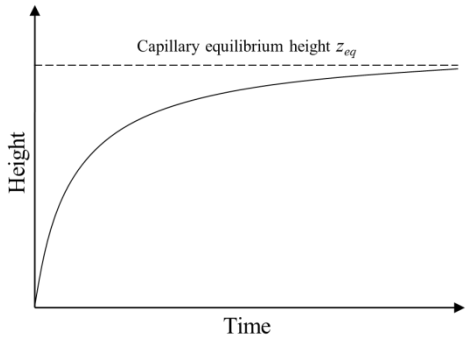

Fig. 2: Schematic view of the flow front evolution during a typical capillary rise experiment through a porous medium.

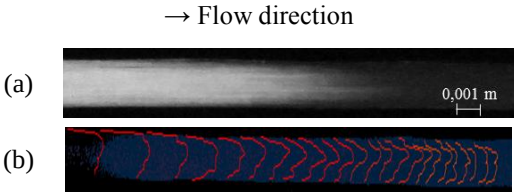

Fig. 3: Capillary flow front tracking inside a fiber bundle with Otsu's algorithm: (a) raw picture of the capillary flow without image post-treatment; (b) successive flow front positions inside a fiber bundle plotted by Matlab.

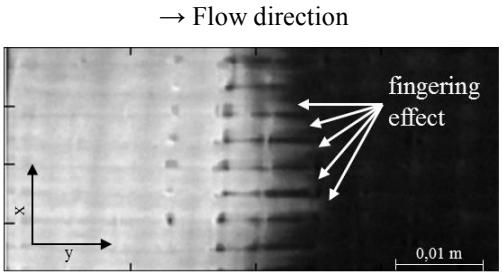

Fig. 4: Visualization of the *"fingering"* effect during capillary rise through glass fiber fabric samples.

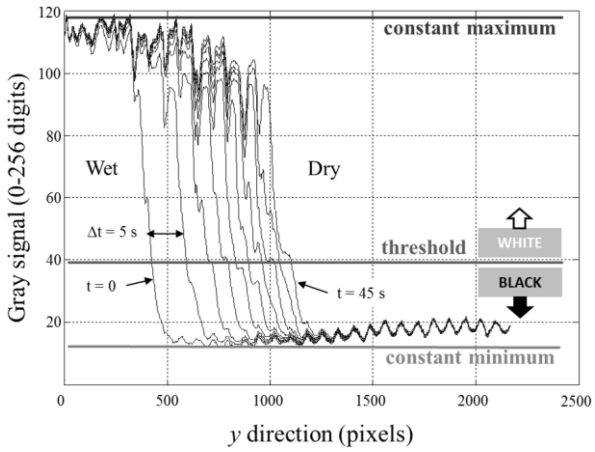

Fig. 5: Graphical analysis of the gray signal from capillary rise images with the threshold value taken for black and white conversion.

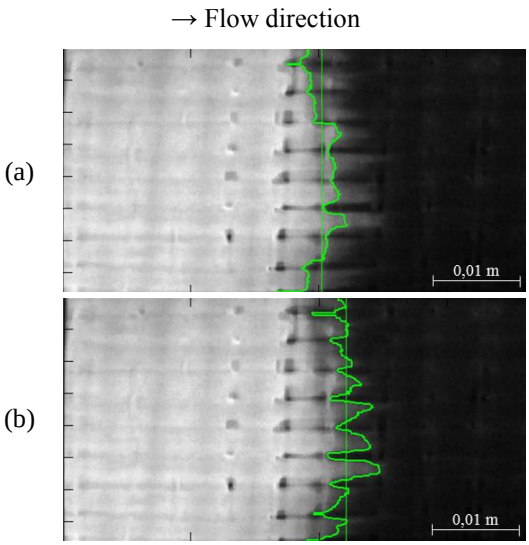

Fig. 6: Detection of the fluid front during capillary rise experiments: (a) with Otsu's algorithm; (b) with the algorithm developed in this investigation.

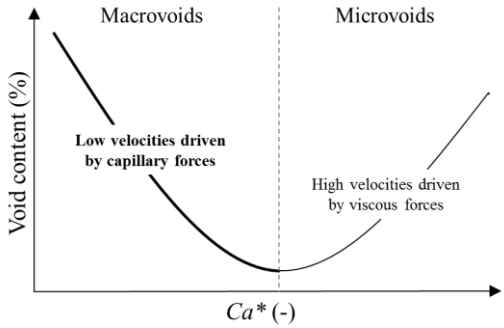

Fig. 7: Theoretical percentage of voids as a function of the injection velocity in composite samples.

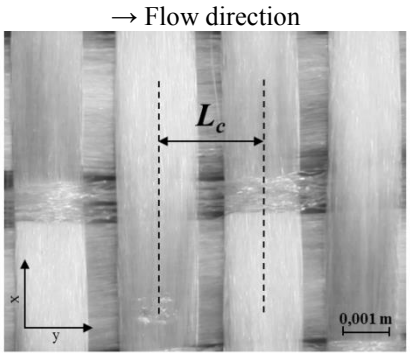

Fig. 8: Characteristic distance L_c between two tows.

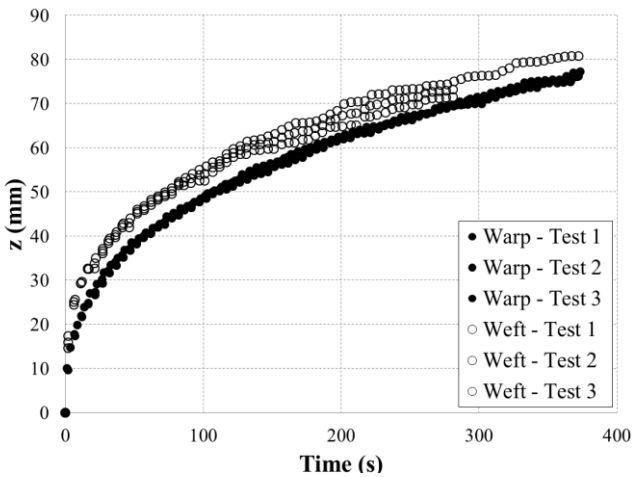

Fig. 9: Height (measured by image analysis) as a function of time. Experimental results of capillary rise tests for JB Martin TG15N NCF fiber glass fabric with hexadecane.

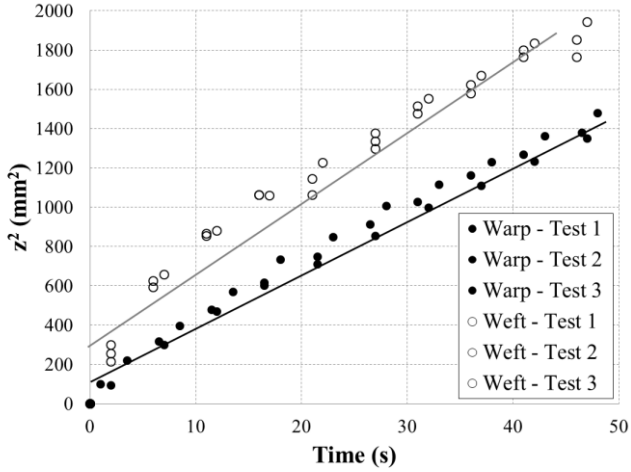

Fig. 10: Square height as a function of time. Validation of *Lucas Washburn* model to determine B_h from capillary rise tests carried out for JB Martin TG15N NCF fiber glass fabric with hexadecane

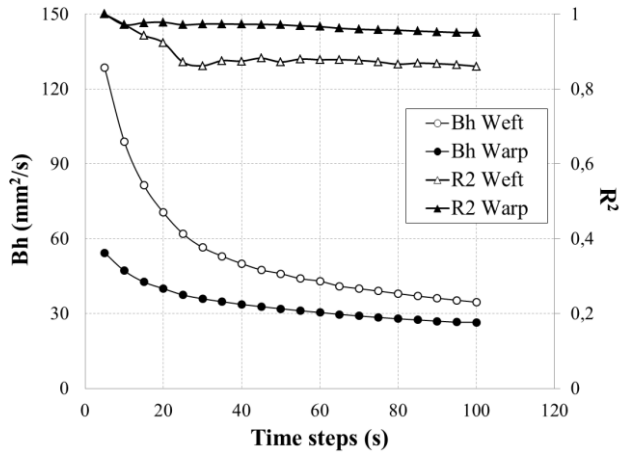

Fig. 11: Evolution of B_h as a function of the number of time steps in the linear regression.

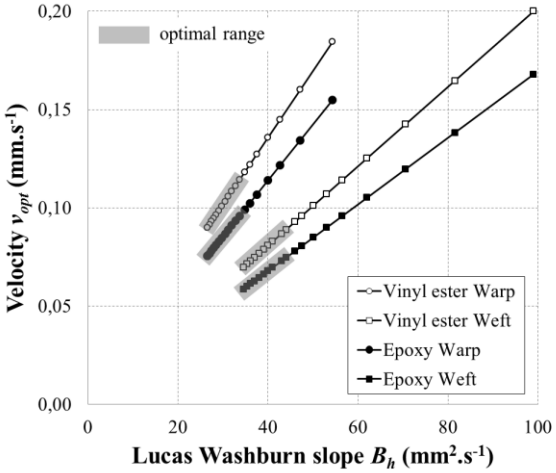

Fig. 12: Optimal injection velocity ranges in the warp and weft directions for vinyl ester and epoxy resins through JB Martin TG15N NCF glass fiber fabric.

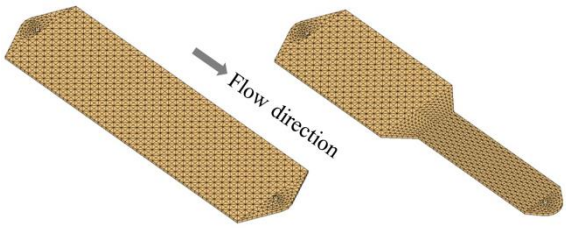

(a) (b)

Fig. 13: Geometry and mesh used for the simulations with PAM-RTM.

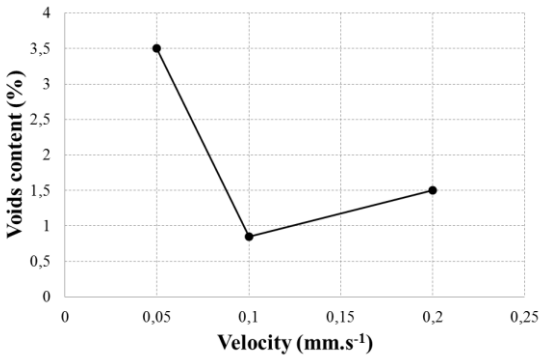

Fig. 14: Void content analysis as a function of the resin velocity. Results obtained for the simulation of section constriction.

Table 1 : Optimal velocity values for hexadecane in JB Martin TG15N NCF fiber glass fabric

	B_h(mm^2.s^{-1})	L_c (mm)	v_{opt} (mm.s^{-1})
Warp	32	1.94	16.5
Weft	45	3.26	13.8

Table 2 : Optimal injection velocity for vinyl ester and epoxy resins through JB Martin TG15N NCF fiber glass fabric

Vinyl ester	v_{opt} (mm.s^{-1})	
	This work	LeBel *et al.*[23]
Warp	0.109	0.077 to 0.18
Weft	0.0909	0.077 to 0.20
Epoxy resin	v_{opt} (mm.s^{-1})	
	This work	LeBel *et al.*[23]
Warp	0.0912	0.06 to 0.14
Weft	0.0763	0.06 to 0.14

Table 3 : Simulations flow conditions and void content analysis in section constriction

velocity		% void	
Large section	Small section	Large section	Small section
v_{opt}	$2\ v_{opt}$	0,85	1,5
$0{,}5\ v_{opt}$	v_{opt}	3,5	0,85
v_{opt}	v_{opt}	0,85	0,85